

probability,  $\epsilon_F(\text{BN})$ , can be obtained from the requirement for diffusion control<sup>11</sup>

$$k_w \cdot d = \epsilon_F(\text{BN}) \cdot c \cdot d/4 > Nu \cdot D \quad (4)$$

where  $c$  is the F-atom mean thermal speed.<sup>‡</sup> Figure 2 illustrates our data and the results predicted by Eq. (3). We use  $D = 0.39 \text{ cm}^2/\text{sec}$  at  $T = 100^\circ\text{C}$ ,  $P = 1 \text{ atm}$  (calculated from Svehla parameters<sup>12</sup>),  $Nu = 3.66$ , and assume  $\eta_D \cdot \eta_{\text{Al}_2\text{O}_3} = 0.93 = \text{constant}$  to compute the values shown by the line. These results show the reaction to be diffusion controlled. Thus, for diffusion limited experiments at or above room temperature, we obtain the useful criterion for complete reaction ( $> 99\%$  F-atom consumption)

$$V[\text{cm}^3 (\text{STP}) / \text{sec}] < 1.6L[\text{cm}]$$

### Discussion

The principle difficulty in the use of F/BN gasification to measure F-atom concentrations is control of sample temperature to avoid  $\text{F}_2$  reaction. This can easily be achieved by limiting BN consumption to less than 0.5% of the specimen, as was the case in most of our experiments. Then the reaction enthalpy cannot heat a specimen initially at room temperature to more than 500K. Temperature control might be more difficult with small BN specimens and higher F-atom concentrations. In this case it would be possible to infer F-atom concentrations from measurements of transient specimen temperature.

The agreement between F-atom concentrations measured by chemiluminescent titration and by reaction with boron nitride leads us to conclude that the present gravimetric method is accurate to at least  $\pm 10\%$ . Atom recombination and production of species other than  $\text{BF}_3$  do not interfere with this method. The  $\text{F}_2/\text{BN}$  reaction may be ignored at room temperature but becomes significant near 500K. This new method permits F-atom concentration measurements above  $\text{ca. } 10^{15} \text{ cm}^{-3}$ , where systematic errors<sup>7</sup> appear in the chemiluminescent titration method. Calibration of spectroscopic techniques and *in situ* measurement of concentration gradients (e.g., in gas dynamic hydrogen fluoride laser nozzles) are other suggested applications of the F/BN gasification reaction.

### References

- Rosner, D.E. and Allendorf, H.D., "Kinetics of the Attack of Refractory Solids by Atomic and Molecular Fluorine," *Journal of Physical Chemistry*, Vol. 75, Feb. 1971, p. 308-317.
- Rosner, D.E. and Allendorf, H.D., "Kinetics of the Attack of Refractory Materials by Dissociated Gases," G.R. Belton and W.C. Worrell, Eds., *Heterogeneous Kinetics at Elevated Temperature*, Plenum, New York, 1970, pp. 231-251.
- Wise, S.S., Margrave, J.L., Feder, H.M., and Hubbard, W.N., "Fluorine Bomb Calorimetry. XVI. The Enthalpy of Formation of Boron Nitride," *Journal of Physical Chemistry*, Vol. 70, Jan. 1966, pp. 7-10.
- Stull, D.R. and Prophet, H., *JANAF Thermochemical Tables*, Second Ed., Nat'l. Stand. Ref. System-NBS Publication 37, U.S. Govt. Printing Office, Washington, D.C., 1971.
- Ganguli, P.S. and Kaufman, M., "The Rate of Homogenous Recombination of Fluorine Atoms," *Chemical Physics Letters*, Vol. 25, March 1974, pp. 221-224.
- Nordine, P.C., "Dissociation Energy of Chlorine Monofluoride," *Journal of Chemical Physics*, Vol. 61, July 1974, pp. 224-226.
- Nordine, P.C. and Rosner, D.E., "Chemiluminescent Titration of  $\text{F(g)}$  with  $\text{Cl}_2(\text{g})$  and Microwave Production of Atomic Fluorine," *Journal of the Chemical Society, Faraday Transactions I*, Vol. 72, June 1976, pp. 1526-1533.
- Foon, R. and Kaufman, M., "Kinetics of Gaseous Fluorine Reactions," *Progress in Reaction Kinetics*, Vol. 8, Feb. 1975, pp. 81-160.
- Nordine, P.C., Rosner, D.E. and Kindlmann, P.J., "New Methods for Studying Gas/Solid Reaction Kinetics Using Automated Resistance Monitoring," *Review of Scientific Instruments*, Vol. 44, July 1973, pp. 821-825.
- Nordine, P.C. and LeGrange, J.D., "Heterogeneous Fluorine Atom Recombination/Reaction on Several Materials of Construction," *AIAA Journal*, Vol. 14, May 1976, pp. 644-647.
- Rosner, D.E., "Convective Diffusion as an Intruder in Kinetic Studies of Surface Catalyzed Reactions," *AIAA Journal*, Vol. 2, April 1964, pp. 593-610.
- Svehla, R.A., *Estimated Viscosities and Thermal Conductivities of Gases at High Temperatures*, NASA Technical Report R-132, 1962.

## On the Application of Tension to Compliant Membranes

James M. McMichael\* and Norman E. Mease†  
National Bureau of Standards, Washington, D.C.

THE feasibility of achieving drag reduction by the use of compliant surfaces in turbulent boundary layers is currently a topic of considerable interest. Although a substantial experimental effort has been reported and significant drag reductions have been noted, the results, to date, have been inconclusive.<sup>1-4</sup> With support of the NASA Langley Research Center, NBS has undertaken to investigate the merits of the compliant surface as an effective method for drag reduction. An important consideration in such an investigation is that the surface motion be adequately specified, and it is necessary, therefore, not only to assure that the tension and membrane mass per unit area be specified but that the applied tension be uniformly distributed and continuously monitored. In addition, the effect of air impedance on the normal modes of the surface motion must also be considered. In the design of an appropriate surface, a method of applying tension that meets these conditions has been developed and evaluated, and it is the purpose of this note to describe the method and the results of this initial evaluation.

A square frame sized to allow a free membrane area 1.24 m on each side was constructed of aluminum angle material. This frame with the membrane attached is to be inserted as a section of a larger boundary-layer plate for use in the wind-tunnel tests on drag reduction. Solid aluminum webs were added at each corner of the frame so as to divide each side of the angle frame into a separate chamber adjoining each edge of the free-membrane area as shown in Fig. 1. Teflon tape was placed along the edges under the membrane to reduce friction. Applying suction equally to opposite chambers of the frame permits the membrane tensions in two directions ( $x$  and  $y$ ) to be adjusted independently by varying suction in the two pairs of opposite chambers. The uniformly distributed chamber pressure, which can be monitored by pressure taps and transducers, enhances uniformity of the tension applied along each edge of the free membrane. This method also has the advantages that tension can be controlled and monitored at a remote station (outside the wind tunnel), and a very smooth membrane surface without wrinkles can be obtained.

The perimeter of the membrane over each chamber is trapezoidal in shape, with an aspect ratio sufficiently large that the tension  $T$  may be computed from an expression for the (approximately uniform) static displacement  $\eta_0$  of the longitudinal centerline of the trapezoid

$$T = \Delta p b^2 / 8\eta_0 \quad (1)$$

Received May 6, 1976; revision received July 14, 1976.

Index categories: Boundary Layers and Convective Heat Transfer—Turbulent; Research Facilities and Instrumentation.

\*Mechanical Engineer, Aerodynamics Section.

†Aerospace Research Engineer, Aerodynamics Section.

‡This condition is met if  $\epsilon_F(\text{BN}) > 0.1$  for these experiments.

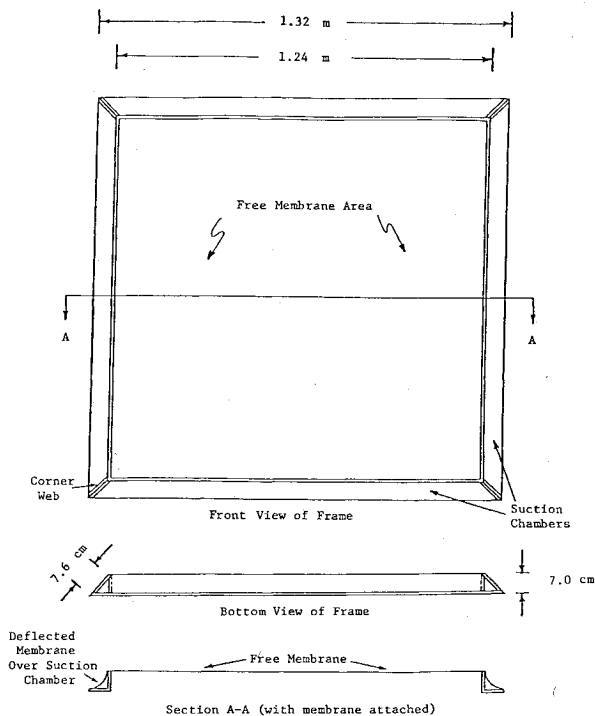


Fig. 1 Support frame for compliant membrane.

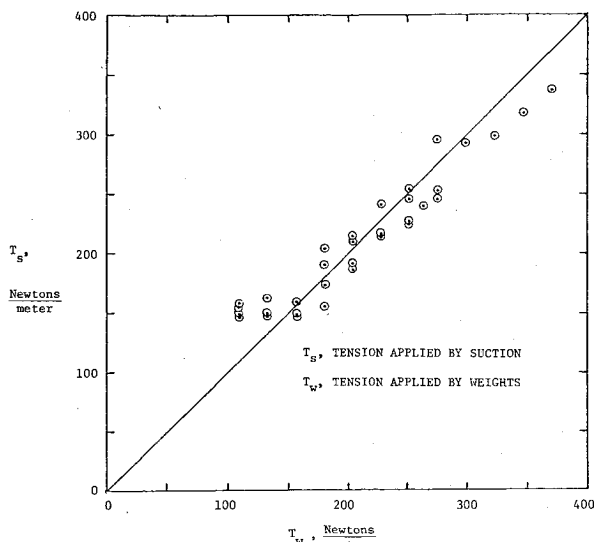
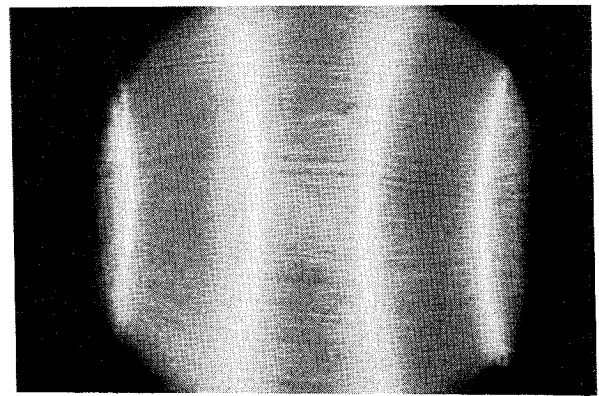


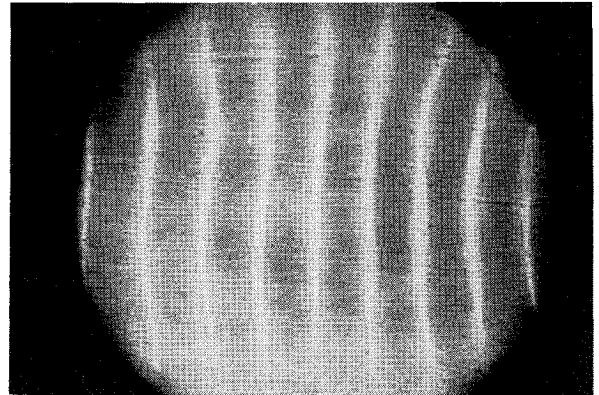
Fig. 2 Direct comparison of tension by suction technique and tension by dead weight.

where  $\Delta p$  is the pressure differential across the membrane and  $b$  is the height of the trapezoid.

To assess the adequacy of Eq. (1) for determining the tension, a 0.025-mm-thick mylar membrane was stretched over the frame and mounted in a vertical plane. Suction was applied to the top chamber while the two side chambers were relaxed ( $T_x = 0$ ), and a system of variable dead weights was attached to a bar clamped to the bottom edge of the membrane. At equilibrium, the tension computed from Eq. (1) for the top edge should balance the tension computed from the distributed dead weights along the bottom edge. Figure 2 shows the measured comparison of the two. The scatter in the data is due to residual friction along the top edge of the membrane where it adjoins the suction chamber. Because of this friction, the tension from Eq. (1) is either higher or lower than the tension applied by the weights,  $T_w$ , depending upon whether  $T_w$  was decreased or increased, respectively, during the tests.



a)  $f = 200$  Hz



b)  $f = 533$  Hz

Fig. 3 Typical standing wave patterns in membrane surface.

The natural frequencies of square membranes vibrating in vacua are given by the equation

$$f_{mn} = K\sqrt{m^2 T_x + n^2 T_y} \quad (2)$$

where  $m$  and  $n$  are the  $x$  and  $y$  modal numbers, respectively, and

$$K = 1/2a\sqrt{\rho h} = 1/2\sqrt{M}$$

where  $\rho$  is the density of the membrane,  $h$  is the membrane thickness,  $a$  is the length of one side of the membrane, and  $M$  is the mass of the free membrane.

A smaller bench-top frame, 0.362 m by 0.362 m, was constructed of the same aluminum angle material as the larger frame to examine the effects of air loading on the frequencies of the normal modes. The fundamental frequency of the tensioned mylar membrane was determined by placing a 30-cm loudspeaker approximately 30 cm behind the membrane as an exciter. The speaker frequency was controlled by a sine wave oscillator. An optical system provided by NASA Langley was used to obtain time exposure photographs of the various standing wave patterns as shown in Fig. 3 for two of the higher modal configurations. The area shown is 30 cm in diameter.

With  $T_x = T_y$ , the fundamental frequency  $f_{11}$  was calculated from Eq. (2) for the membrane tensioned by suction using the values of  $T$  computed from Eq. (1) and compared to the fundamental frequencies obtained with the loudspeaker exciter. A similar comparison was made for the same membrane tensioned by distributed dead weights with  $T_x = 0$ . The data in both cases indicate that  $f_{11}$  computed from Eq. (2) is approximately 3.5 times greater than the observed values over the tension range examined (from 28 to 220 Newtons per meter). This frequency shift is believed to be due to acoustical impedance of air surrounding the membrane.

A further demonstration of the effect of air loading on the frequencies of the natural modes is presented in Fig. 4 in which the frequencies measured for a number of higher modal configurations are compared to the frequencies predicted by

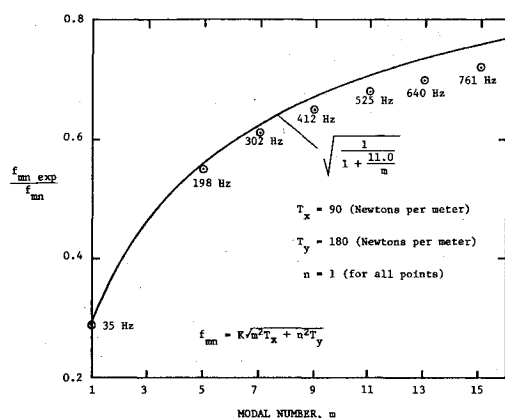


Fig. 4 Effect of air impedance with increasing frequency.

Eq. (2) in the case in which  $n = 1$  and  $m$  is varied from 1 to 15. Assuming that the factor  $K$  in Eq. (2) can be corrected for air impedance by writing

$$K' = 1/2\sqrt{(M + M_a)}$$

where  $M$  is the mass of the membrane and  $M_a$  is the effective added mass of air, the frequency ratio shown is expressible as  $K'/K$  where

$$K'/K = \sqrt{M/(M + M_a)}$$

If the added mass is assumed to be proportional to the wavelength  $\lambda$  of the standing wave, where  $\lambda = 2a/m$ , then

$$K'/K = 1/\sqrt{1 + c/m} \quad (3)$$

where  $c$  is a constant. Matching this expression to the experimentally determined frequency ratio for  $m = 1$ , the value of  $c$  is found to be 11.0. Equation (3), as shown in Fig. 4, is in reasonable agreement with the trend of the measured frequency ratios.

### References

- <sup>1</sup>Blick, E.F., Walters, R. R., and Smith, R., "Compliant Coating Skin Friction Experiments," AIAA Paper 69-165, New York, 1969.
- <sup>2</sup>Lissaman, P. B. S. and Harris, G. L., "Turbulent Skin Friction on Compliant Surfaces," AIAA Paper 69-164, New York, 1969.
- <sup>3</sup>McAlister, K. W. and Wynn, T.M., "Experimental Evaluation of Compliant Surfaces at Low Speeds," NASA TM X-3119, 1974.
- <sup>4</sup>Ash, R. L. and Bushnell, D. M., "Compliant Wall Turbulent Skin-Friction Reduction Research," AIAA Paper 75-833, 1975.
- <sup>5</sup>Morse, P. M., "Vibration and Sound," McGraw-Hill, New York 1948, pp. 332-333.

## Anisotropic Radiatively Coupled Wedge Flow

James B. Elgin\* and Judson R. Baron†  
Massachusetts Institute of Technology,  
Cambridge, Mass.

### Introduction

GEOMETRICALLY thin shock layers are advantageous in reducing the radiation heat transfer to a high-speed body. Gibeling and one of the present authors<sup>1</sup> have shown,

Received May 20, 1976. Supported by the U.S. Air Force Office of Scientific Research under Contract F44620-75-C-0040.

Index categories: Radiatively Coupled Flows and Heat Transfer; Radiation and Radiative Heat Transfer; Supersonic and Hypersonic Flow.

\*Research Assistant. Presently at Aerodyne Research, Inc., Bedford, Mass.

†Professor, Department of Aeronautics and Astronautics.

in fact, that optimum two-dimensional bodies for minimizing the overall radiant heat transfer correspond closely to those associated with reductions in the disturbed volume of air when the field is radiatively coupled. However, elongated shock layers imply anisotropic radiation fields. Therefore, the differential [Milne-Eddington (*M.E.*)] approximation used in Ref. 1 is somewhat questionable.

In the optically thin limit for which emission dominates and reabsorption is negligible, a purely differential description is appropriate. Wedge flow results have been carried out for that limit by Jischke<sup>2</sup> using an integral method, and Olfe<sup>3</sup> based on an expansion in shock density ratio.

Recently, an extension of the Milne-Eddington has been proposed and evaluated.<sup>4,5</sup> The essential improvement was the introduction of variable closure for the higher moments of the intensity distribution (or equivalently for a higher-order spherical harmonics expansion) based on ellipsoidal intensity distribution modeling. The inadequacy of *M.E.* to represent anisotropic radiation fields was shown there by means of comparisons of exact, variable closure, and *M.E.* evaluations for several representative regions. These included quite thin ( $10^\circ$ - $170^\circ$ ) rhombic section prisms, and concentric annular regions between cylinders and cones, all being representative of shock-layer regions. Geometric corners imply a most severe test for radiative approximations of a differential nature. *M.E.* showed marked departures from the exact values for flux and intensity in such regions, but the variable closure ellipsoids gave rather good agreement. This suggests the utility of ellipsoidal modeling for both anisotropic and coupled fields. The purpose here is an application of the concept to a radiatively coupled wedge flow, which is a reference case considered in Ref. 1 and provides a realistic basis for examination of *M.E.* adequacy for shock layers.

### Analysis

The fluid field is specified by an integral method and, consistent with this, the radiation intensity is specified by an assumed distribution across the shock layer. For an inviscid, perfect-gas continuum, the radiation contribution to the fluid field description<sup>6,7</sup> is the nonadiabatic flux divergence term

$$\nabla \cdot \bar{q} = \alpha(4\sigma T^4 - I_0) \quad (1)$$

in the energy balance. Here,  $\alpha$  is a temperature-dependent grey gas absorption coefficient<sup>5</sup> and  $I_0$  is the zeroth angular moment of intensity, i.e.,  $\int_{4\pi} I d\Omega$ . Significantly, only the lowest order moment is required explicitly since the absorption process is independent of the photon direction of travel through a point.

Although coupled to the fluid field, it proves convenient to consider  $I_0$  as a parametric function of the problem and proceed iteratively based on an initial assumption of  $I_0 \equiv 0$ . The physical rationale is an increasing absorption with successive iteration cycles. Since the energy loss from each fluid element during a given cycle is greater than would be expected with full reabsorption, the temperature level for each cycle is too small. Corresponding radiation moments then are based on lower emission levels and a uniformly lower  $I_0$  increases monotonically with iteration cycle. The essential advantage is a separation of radiation and fluid-field evaluations; the adequacy of the converged solution depends upon the accuracy of the basis for  $I_0$ .

Since field points located away from the boundaries are irradiated over relatively larger solid angles, an  $I_0$  maximum is to be anticipated between the surface and shock. Assuming a parabolic distribution of the form

$$I_0(x, y) = I_{00}(x) + I_{01}(x)(y/\delta) + I_{02}(x)(y/\delta)^2 \quad (2)$$

implies the need for  $I_0$  at  $y = 0$ ,  $(\delta/2)$ , and  $\delta$ ; i.e., in Eq. (2)

$$I_{0i} = a_i I_0(x, 0) + b_i I_0(x, (\delta/2)) + c_i I_0(x, \delta) \quad (3)$$